

# Theoretical study of opacity for a mixture of gold and gadolinium at a high temperature

Jun Yan<sup>1,2</sup> and Yu-Bo Qiu<sup>1</sup>

<sup>1</sup>*Institute of Applied Physics and Computational Mathematics, Beijing 100088, China*

<sup>2</sup>*Center of Atomic and Molecular Physics, Tsinghua University, Beijing 100084, China*

(Received 15 March 2001; published 9 October 2001)

Using the detailed configuration accounting with the term structures treated by the unresolved transition array model, we have presented a method to calculate the spectral-resolved opacity for high temperature and density plasmas. Due to the fully relativistic treatment, incorporated with the quantum defect theory to handle the huge number of transition arrays from configurations with high principal quantum number, we can calculate the opacity of any medium- and high- $Z$  plasmas conveniently. In the present work, the frequency-dependent opacity and the Rosseland mean opacity are calculated for a mixture of gold and gadolinium at a high temperature, 250 eV, and three densities, 0.1 g/cm<sup>3</sup>, 1.0 g/cm<sup>3</sup>, and 10.0 g/cm<sup>3</sup>. Agreement between our theoretical results and experimental measurements and other theoretical simulations is obtained.

DOI: 10.1103/PhysRevE.64.056401

PACS number(s): 52.25.Os, 32.90.+a, 52.25.Vy

## I. INTRODUCTION

In the indirect approach to the inertial confinement fusion (ICF) [1,2], the radiation that drives the implosion of the fuel capsule is generated by the interaction of intense beams with the interior wall of a high- $Z$  cavity, or a hohlraum. In order to reduce the radiation energy lost to the walls of the hohlraum and increase the efficiency with which the radiation couples with the capsule, materials with high Rosseland mean opacity should be used. Hence for a given laser power (and x-ray conversion efficiency) the drive temperature increases as does the coupling efficiency of the radiation to the fuel pellet. Typically, people use pure Au hohlraums heated to a temperature of  $\sim 250$  eV. There are significant windows in the frequency-dependent opacity of Au, which dominates and reduces the Rosseland mean opacity. In order to improve the Rosseland mean opacity, people try to use hohlraums of mixture materials, which can overlap the windows of frequency-dependent opacity by each other. Recently, Orzechowski and co-workers measured the Rosseland mean opacity of a mixture of Au and Gd at high temperatures [3]. Theoretical simulation [3] was also carried out using the XSN opacity model [4] in their work.

Theoretical calculations of plasma opacity require a huge number of atomic data. For low- $Z$  plasmas, some works [5,6] have been presented with detailed calculations and a large amount of computational efforts. However, such detailed analyses become impractical for high- $Z$  plasmas. People usually use various statistical methods, such as the average atom (AA) model [7]. Because of line overlapping and line broadening of spectra from a huge number of transition arrays in various ionic stages, unresolved spectra are often observed in laser-produced high- $Z$  plasmas. The unresolved transition array (UTA) model [8] is an efficient approach to describe such unresolved spectral structures. Based on the UTA, the supertransition array (STA) [9] method has been developed and proved to be a powerful tool in calculation of opacity for high- $Z$  materials. The occurrence of high principal quantum numbers in hot dense local thermodynamic equilibrium (LTE) plasmas leads to a huge number of configurations. Quantum defect theory (QDT) [10–14] is a powerful method

to treat these configurations. In this method, the physical quantities show smooth properties and can be treated in a unified manner within channels [15]. Therefore, we can perform interpolations (rather than extrapolations) to reduce computational efforts. With these features in our method, we have developed a computational code [16–19] to calculate the spectral-resolved opacity of plasmas. The method can conveniently be used to calculate the opacity of any medium- and high- $Z$  plasma at high temperature and density. Good agreements were obtained between our theoretical simulations of the transmission spectra and the corresponding benchmark experimental measurements in our previous work [16–18]. In the present work, the frequency-dependent opacity and the Rosseland mean opacity are calculated for a mixture of gold and gadolinium at a high temperature, 250 eV, and three densities, 0.1 g/cm<sup>3</sup>, 1.0 g/cm<sup>3</sup>, and 10.0 g/cm<sup>3</sup>. Agreement between our theoretical results and experimental measurements and other theoretical simulations is obtained.

## II. THEORETICAL METHOD

The Rosseland mean opacity [20] is used to describe radiation transport in optically thick materials when the matter and radiation are in thermodynamic equilibrium. It is defined as a weighted harmonic mean of the energy dependent opacity,

$$\frac{1}{\kappa_R} \equiv \frac{\int_0^\infty \kappa_\nu^{-1} (\partial B_\nu / \partial T) d\nu}{\int_0^\infty (\partial B_\nu / \partial T) d\nu}, \quad (1)$$

where  $T$  is the material and radiation temperature,  $B_\nu$  is the black body spectrum, and  $\kappa_\nu$  is the frequency-dependent opacity. This mean opacity is dominated by the low opacity regions of the frequency-dependent opacity. In the configuration average approximation, the frequency-dependent opacity can be written as [21]

$$\kappa(\hbar\omega)\rho = \sum_i \left[ \sum_{c,c'} N_{i,c} \sigma_{i,c,c'}^{bb}(\hbar\omega) + \sum_c N_{i,c} \sigma_{i,c}^{bf}(\hbar\omega) \right] + N_e \sigma^{ff}(\hbar\omega), \quad (2)$$

where  $\rho$  is the plasma density,  $i$  indicates the ionic stage,  $N_{i,c}$  is the number of ions of configuration  $c$  per unit volume,  $N_e$  is the number of electrons per unit volume,  $\sigma_{i,c,c'}^{bb}(\hbar\omega)$  is the photoexcitation cross section from configuration  $c$  to  $c'$ ,  $\sigma_{i,c}^{bf}(\hbar\omega)$  is the total photo-ionization cross section from all subshells of configuration  $c$ , and  $\sigma^{ff}(\hbar\omega)$  is the free-free absorption cross section, which can be calculated by the simple Kramer's formula with Gaunt factor. Therefore the crucial problem of the frequency-dependent opacity calculation is to obtain the population density and the cross sections of photoexcitation and photoionization processes.

The population density can be obtained by solving the well-known Boltzmann-Saha equations for the LTE plasmas. The key point is to include important configurations as much as possible in the opacity calculation. Here we use the self-consistent-field energy levels database to investigate and produce important configurations. Therefore, the most important configurations are included in solving Boltzmann-Saha equations and in the calculations of properties of photoexcitation and photoionization processes.

The configuration-to-configuration transitions are treated in the UTA approximation [8,9]. The photoexcitation and photoionization cross sections are calculated from the one-electron properties. In the configuration average approximation, the photoexcitation cross section can be written as

$$\sigma_{i,c,c'}^{bb}(\hbar\omega) = \frac{\pi h e^2}{m c} f_{i,c,c'} \mathcal{L}(\hbar\omega), \quad (3)$$

where  $f_{i,c,c'}$  is the configuration average oscillator strength and  $\mathcal{L}(\hbar\omega)$  is the line shape function. In general, the observed spectral profile is a convolution of Gaussian and Lorentzian profiles. If the transition energy is assumed to be approximately the same for all lines of the transition array, the relation of  $f_{i,c,c'}$  to the single-electron transition oscillator strength  $f_{\alpha\rightarrow\beta}$  is

$$f_{i,c,c'} = q_\alpha \left( 1 - \frac{q_\beta}{g_\beta} \right) f_{\alpha\rightarrow\beta}, \quad (4)$$

$$f_{\alpha\rightarrow\beta} = \frac{2m}{\hbar \omega g_\alpha} \frac{1}{2k+1} |\langle \alpha || T || \beta \rangle|^2, \quad (5)$$

where  $\hbar\omega$  is the photon energy,  $q_\alpha, q_\beta$  are the occupation numbers of orbital  $\alpha, \beta$ , respectively,  $k$  is the rank of electric multipoles,  $g_\alpha$  is the statistical weight for initial orbital  $\alpha$ , and  $\langle \alpha || T || \beta \rangle$  is the bound-bound reduced transition matrix element [22].

The photoionization cross section for configuration  $c$  of ionic stage  $i$  can be written as

$$\sigma_{i,c} = \frac{\pi h e^2}{m c} \sum_\alpha q_\alpha \frac{d f_\alpha}{d \varepsilon}, \quad (6)$$

where the summation runs over all subshells of the configuration.  $d f_\alpha / d \varepsilon$  is the density of oscillator strength given by

$$\frac{d f_\alpha}{d \varepsilon} = \frac{2m}{3 \hbar \omega g_\alpha} |\langle \alpha || T || \tilde{\varepsilon} \rangle|^2, \quad (7)$$

where  $\langle \alpha || T || \tilde{\varepsilon} \rangle$  is the energy-normalized transition-matrix element from the initial bound orbital state  $\alpha$  to the continuum orbital state  $\tilde{\varepsilon}$  [22].

According to QDT, the photoexcitation and photoionization processes can be treated in a unified manner. The infinite bound and adjacent continuum states with the same angular momentum and parity can form a channel in which the quantum defects  $\mu$  vary smoothly [15,23] with the excitation energy. We can define the energy-normalized matrix elements for the photoexcitation as

$$\langle \alpha || \tilde{T} || \beta \rangle = N_\beta \langle \alpha || T || \beta \rangle, \quad (8)$$

where  $N_\beta^2 = \nu_\beta^3 / (Z_i + 1)^2$  is the density of the final state,  $Z_i$  is the ionization degree, and  $\nu_\beta = n - \mu_\beta$  is the effective principal quantum number of the final state. This energy-normalized matrix element also varies smoothly across the ionization threshold. Therefore, with several benchmark points, the relevant transition matrix elements from an initial state to the final channel can be obtained conveniently by interpolation. Furthermore, the UTA parameters, i.e., the UTA configuration average transition energy and UTA line-width, depend only on the radial Slater integrals, which also have good channel behavior. Therefore, we can calculate not only photoionization and photoexcitation cross sections but also UTA parameters with much less computational efforts.

### III. RESULTS AND DISCUSSION

Based on the theoretical method described above, we have developed a computer code to provide opacity data for high temperature and density medium- and high- $Z$  plasmas. As mentioned in the Introduction, in the indirect drive approach to ICF, increasing the Rosseland mean opacity cannot only reduce the radiation energy loss to the walls of the hohlraum, but also increase the coupling efficiency between the radiation and fuel capsule. This can raise the temperature of the laser heated hohlraum for a given laser power, or for a given desired driven temperature, less laser energy is required. Since it is important in ICF, we carry out calculations of opacity for mixture materials and investigate the way to improve the Rosseland mean opacity by blending in materials. Recently, Orzechowski and co-workers presented their experimental measurements of the Rosseland mean opacity of a mixture of Au and Gd at high temperatures, as well as the theoretical results at a temperature of 250 eV and a density of 1.0 g/cm<sup>3</sup>. In the following, we will show our calculated opacity of the mixture of Au and Gd at the temperature 250 eV and three densities 0.1 g/cm<sup>3</sup>, 1.0 g/cm<sup>3</sup>, and 10 g/cm<sup>3</sup>. In each calculation, about 200 000 or much more

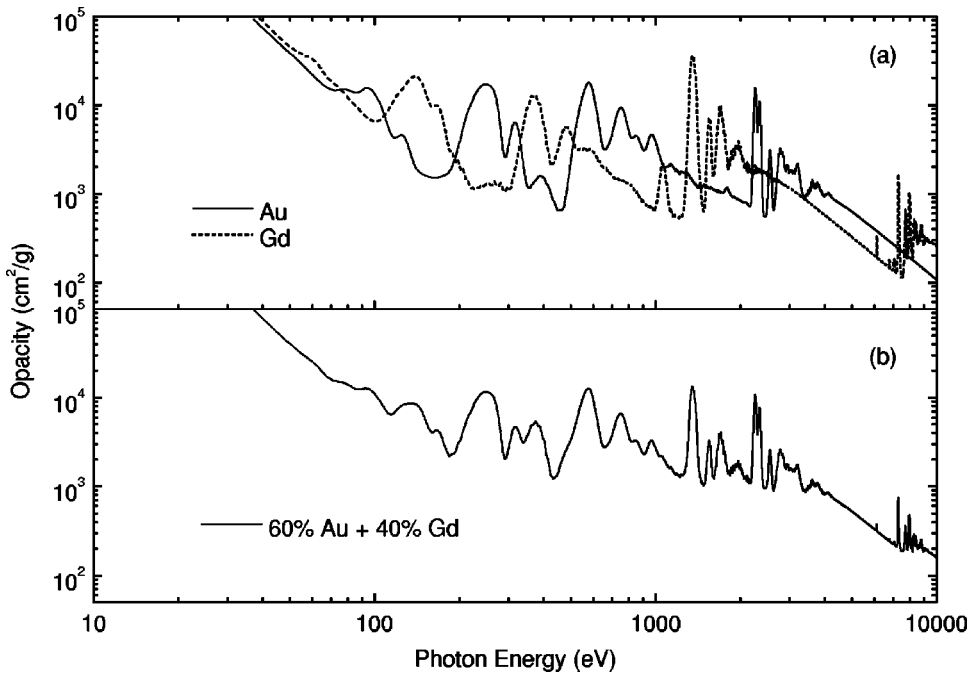


FIG. 1. Frequency-dependent opacity of Au, Gd, and the 60/40 mixture of Au/Gd.

configurations are included, which ensure the convergence of the calculation.

Figure 1 displays the calculated frequency-dependent opacity of Au, Gd and a 60/40 mixture of Au/Gd at a temperature 250 eV and a total density 1.0 g/cm<sup>3</sup>. As can be seen from Fig. 1(a), the windows of the frequency-dependent opacity of Au at about 160 eV, 400 eV, and 1000–2500 eV are overlapped to some extents by the peaks of Gd. Because the Rosseland mean opacity is dominated by the low opacity region, such overlapping can increase the Rosseland opacity: our calculation gives  $\kappa_R=1700$  cm<sup>2</sup>/g for Au,  $\kappa_R=1300$  cm<sup>2</sup>/g for Gd, and  $\kappa_R=2200$  cm<sup>2</sup>/g for the 60/40 mixture of Au/Gd in Fig. 1(b).

Figures 2(a)–2(c) display our calculated Rosseland mean opacities of the Au/Gd mixture at a temperature 250 eV and three densities of 0.1 g/cm<sup>3</sup>, 1.0 g/cm<sup>3</sup>, and 10.0 g/cm<sup>3</sup>, respectively. These mean opacities have been normalized to those of pure Au, i.e.,  $\kappa_R=970$  cm<sup>2</sup>/g of 0.1 g/cm<sup>3</sup>,  $\kappa_R=1700$  cm<sup>2</sup>/g of 1.0 g/cm<sup>3</sup>, and  $\kappa_R=2400$  cm<sup>2</sup>/g of 10.0 g/cm<sup>3</sup>. Experimental results of Orzechowski *et al.* are also given for comparison [3], as well as their predictions using the XSN opacity model [3] and the simulation of the STA method by Colombant *et al.* [24] at the density 1.0 g/cm<sup>3</sup> in Fig. 2(b). XSN simulation results are about 10–12 % higher than the measurements. This discrepancy, as pointed out in Ref. [3], may come from the relative simple

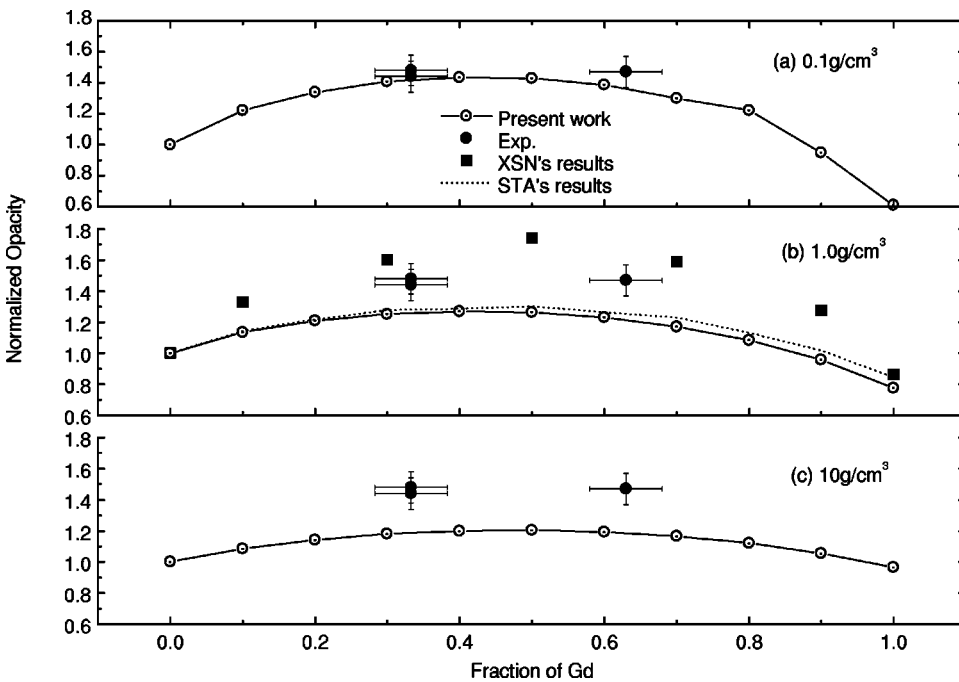


FIG. 2. Rosseland mean opacities of composite normalized to those of pure Au at the temperature 250 eV and three densities 0.1 g/cm<sup>3</sup>, 1.0 g/cm<sup>3</sup>, and 10.0 g/cm<sup>3</sup>. The open points correspond to our theoretical results; the solid points represent the experimental measurements [3]; the solid squares show the theoretical predictions of XSN mode [3]; the dotted line displays the theoretical results of STA (LTE) [24].

treatment of bound-bound transitions in the XSN calculation. In our theoretical method, the bound-bound transitions are calculated carefully. In our previous works [16–18], good agreements were obtained between our theoretical simulations of the spectral-resolved opacity and corresponding experimental benchmark measurements. This also suggested the reliability of our treatments of bound-bound transitions. In the present calculation, the bound-bound transitions from  $1s, 2s, 2p_-, 2p_+, \dots, 5f_-, 5f_+$  initial orbitals to “all” final orbitals ( $n_{max}=10$ ) for each configuration are taken into account. The present calculations give the maximum improvements in the opacity (compared to that of pure Au in the same conditions): a factor of 1.44 (60/40 mixture of Au/Gd), a factor of 1.27 (60/40 mixture), and a factor of 1.21 (50/50 mixture) for three densities of  $0.1 \text{ g/cm}^3$ ,  $1.0 \text{ g/cm}^3$ , and  $10.0 \text{ g/cm}^3$ , respectively. In Fig. 2(b), our calculated Rosseland mean opacities are lower than both experimental measurements and XSN simulations, and agrees very well with STA results; it is more lower than measurements for the case of density  $10.0 \text{ g/cm}^3$  in Fig. 2(c); while for the case of density  $0.1 \text{ g/cm}^3$ , as can be seen in Fig. 2(a), the agreement between our theoretical results and experimental measurements is very good. Because the experiment samples a range of densities and temperatures in reality, our theoretical simulations suggest, if only judged by the improvement of the Rosseland mean opacity, that plasma at densities lower than  $1.0 \text{ g/cm}^3$  may play a more important role in the measurements of the Rosseland mean opacity by Orzechowski *et al.* [3].

In the work of Orzechowski *et al.* [3], the results calculated using the AA model [25] were also given. For the AA model, the calculated Rosseland mean opacity of Au is  $823 \text{ cm}^2/\text{g}$  and  $1390 \text{ cm}^2/\text{g}$  for a 50/50 mixture of Au and Gd. Compared with the experimental measurement, obviously the AA model is quite simple and the results, not only the feature of frequency-dependent opacity, but also the Rosseland mean opacity of pure Au and that of the increase due to blending with Gd, are not very satisfactory. Therefore, more sophisticated opacity models, such as XSN, STA, detailed configuration accounting (DCA) with UTA treatment as the present method, and even more sophisticated methods of DCA and detailed line accounting (DLA) models, are needed for these kinds of problems. Since no detailed descriptions of the XSN model are given in the work of Orzechowski *et al.* [3], and no calculations based on DCA or DLA models are reported (maybe owing to the large amount of computational efforts), we here would like to discuss more about the STA method and our DCA/UTA method in the following text.

Both STA and our methods calculate the transition arrays based on the UTA approximation: This determines that the two methods are at a similar level and can reveal the internal structure of an array when it exists. In the STA method, though superconfiguration is used, through obtaining the convergence with increasing number of STA’s and calculating with each superconfiguration’s own accurate parametric potential, the STA method can almost reproduce the UTA structure exactly. In the present work, we calculate the wave functions, transition arrays, and UTA parameters of each relativistic configuration based on Dirac-Slater potentials. In some cases, our method can provide better agreement with the spectra-resolved experimental measurements [16–18]. While for some cases, especially for  $\delta n=0$  transitions, where configuration interaction (CI) effects are important, the STA method can obtain better results because the CI effects were taken into account more recently [26]. The present work has not taken into account the CI effects yet. Another different treatment is that in the STA method, the frequency-dependent opacities of each element are calculated with the same temperature and effective densities via the same chemical potentials, and then the opacity of mixtures are calculated using their postprocessed program MIX [24]. In the present work, the opacities of the mixture are calculated directly. These two treatments, as our study, should affect very little the opacities of mixture. Anyway, the present theoretical simulation are rather simple for assuming one specific density and temperature when studying the complicated experimental process like the measurement of the heat wave [3]. Detailed theoretical studies with more sophisticated physical considerations, like Orzechowski and co-workers did using the rad-hydro code LASNEX [3], are still needed in order to simulate the experiment more accurately.

Finally, we would like to conclude as follows: with much less computational efforts, our computer code can provide spectral-resolved LTE opacity data with adequate accuracy. The frequency-dependent opacity and the Rosseland mean opacity are calculated for a mixture of gold and gadolinium. Good agreements between our theoretical results and experimental measurements and other theoretical simulations are obtained.

#### ACKNOWLEDGMENTS

We thank Professor Yun-Sheng Li and Professor Jia-Ming Li for helpful discussions. This work is supported by the National Science Foundation of China (Grant No. 10074062), and it is also partially supported by National High-Tech ICF committee of China, Science and Technology Funds of CAEP (Grant No. 20010218).

- 
- [1] J.D. Lindl, R.L. McCrory, and E.M. Campbell, *Phys. Today* **45** (9), 32 (1992).  
 [2] J.H. Nuckolls, L. Wood, A. Thiessen, and G.B. Zimmerman, *Nature (London)* **239**, 129 (1972).  
 [3] T.J. Orzechowski, M.D. Rosen, H.N. Kornblum, J.L. Porter, L.J. Suter, A.R. Thiessen, and R.J. Wallace, *Phys. Rev. Lett.*

**77**, 3545 (1996).

- [4] W.A. Lokke and W.H. Grasberger, Lawrence Livermore National Laboratory Report No. UCRL-52276, 1977.  
 [5] J. Abdallah and R.E.H. Clark, *J. Appl. Phys.* **69**, 23 (1991).  
 [6] F.J. Rogers and C.A. Iglesias, *Astrophys. J., Suppl.* **79**, 507 (1992).

- [7] B.F. Rozsnyai, Phys. Rev. A **5**, 1137 (1972).
- [8] C. Bauche-Arnoult, J. Bauche, and M. Klapisch, Phys. Rev. A **20**, 2424 (1979); **25**, 2641 (1982); **30**, 3026 (1984); **31**, 2248 (1985).
- [9] A. Bar-Shalom, J. Oreg, W.H. Goldstein, D. Shvarts, and A. Zigler, Phys. Rev. A **40**, 3183 (1989); Phys. Rev. E **51**, 4882 (1995).
- [10] M.J. Seaton, Proc. Phys. Soc. London **88**, 801 (1966); Rep. Prog. Phys. **46**, 167 (1983).
- [11] U. Fano, Phys. Rev. A **2**, 353 (1970); J. Opt. Soc. Am. **65**, 979 (1975).
- [12] C.M. Lee and J.-M. Li, Phys. Rev. A **10**, 584 (1974); Acta Phys. Sin. **29**, 419 (1980).
- [13] C. Greene, U. Fano, and G. Strinati, Phys. Rev. A **19**, 1485 (1979).
- [14] J. Yan, Y.-Z. Qu, L. Voky, and J.-M. Li, Phys. Rev. A **57**, 997 (1998).
- [15] J.-G. Wang, X.-M. Tong, and J.-M. Li, Acta Phys. Sin. **45**, 13 (1996).
- [16] J. Yan, Y.-Z. Qu, and J.-M. Li, High Power Laser and Particle Beams **11**, 65 (1999).
- [17] J. Yan and J.-M. Li, Chin. Phys. Lett. **17**, 194 (2000).
- [18] J.-M. Li, J. Yan, and Y.-L. Peng, Radiat. Phys. Chem. **59**, 181 (2000).
- [19] Y.-L. Peng, X.-Y. Han, J.-M. Li, Y.-N. Ding, J.-M. Yang, and Z.-J. Zheng, Science (to be published).
- [20] S. Rosseland, Mon. Not. R. Astron. Soc. **84**, 525 (1924).
- [21] D. Kilcrease, J. Abdallah, Jr., J. Keady, and R.E.H. Clark, J. Phys. B **26**, L717 (1993).
- [22] Z.-X. Zhao and J.-M. Li, Acta Phys. Sin. **34**, 1469 (1985); L. Liu and J.-M. Li, *ibid.* **42**, 1901 (1993).
- [23] J.-G. Wang, Y.-Z. Qu, and J.-M. Li, Phys. Rev. A **52**, 4274 (1995).
- [24] D. Colombant, M. Klapisch, and A. Bar-Shalom, Phys. Rev. E **57**, 3411 (1998).
- [25] Jon T. Larsen, in *Radiative Properties of Hot Dense Matter: Proceedings of the Fourth International Workshop*, edited by W. Goldstein, C. Hopper, J. Gauthier, J. Seely, and R. Lee (World Scientific, Singapore, 1990).
- [26] A. Bar-Shalom, J. Oreg, M. Klapisch, and T. Lehecka, Phys. Rev. E **59**, 3512 (1999).